Proceedings of the 26th International Conference on Offshore Mechanics and Arctic Engineering
OMAE2007
June 10-15, 2007, San Diego, California, USA

OMAE2007-29150

CFD TRUSS SPAR HULL BENCHMARKING STUDY

Owen H. Oakley, Jr.
Chevron Energy Technology Company

Yiannis Constantinides
Chevron Energy Technology Company

ABSTRACT

Blind comparisons of computational fluid dynamics (CFD) predictions are made against large scale experiments of a truss spar hull. The overall objective of the work is to try and mature CFD modeling capability related to motion and loads for offshore platforms. Specific goals include the testing of newly developed meshing techniques and seeking an understanding of how spar appurtenances interact.

The key comparisons are illustrated in comparisons of the simple case of a spar hull with strakes alone against a second, far more complex case, involving multiple appurtenances. The latter exhibits very different vortex induced motion (VIM) behavior. The CFD predictions were made with knowledge of the as-built model details, but without access to the experimental results. The estimates were found to be in close agreement with the experiments or slightly conservative. We continue to observe that the better the model fidelity, the better will be the comparison with the benchmark. The computations show that high quality predictions are now feasible, given access to sufficient computational hardware and accurate meshing of the body in question.

BACKGROUND

It has become increasingly clear in the last decade that model scale experiments of the vortex induced motion of spars is critically dependent on the geometric details, specifically the pipes, chains and anodes that are commonly found on the external hull. These small scale appurtenances presumably interact with the boundary layer and affect the point of separation. This in turn controls the vortex shedding character, their correlation along the hull and the resulting VIM amplitude. Since the boundary layer thickness is strongly dependent on the Reynolds number (Re), there was serious concern about the interaction of the appurtenances with the boundary layer and the validity of small scale tests.

During this period, computational fluid dynamic (CFD) modeling capability had matured [1]. While comparisons with model tests appeared encouraging, unexplained deviations hindered acceptance of CFD as a reliable design and analysis tool. One explanation suggested was the typical lack of similitude between the CFD model and the benchmark experiment. “Minor” geometric details were often ignored for computational expediency. In order to address this, methods were developed for the generation of meshes of increasing geometric complexity that would make the computations accurate, yet relatively efficient to run [2]. Suitable benchmark data was still lacking.

In order to answer these modeling questions, an experimental program of study was initiated to investigate the role of appurtenances on the VIM of spars as a function of Re. High Re tests were performed at the Carderock Division of the Naval Surface Warfare Center, Bethesda, MD, also known as the David Taylor Model Basin (DTMB). CFD runs were conducted to aid in the planning of these high blockage tests. These tests provide an ideal benchmarking opportunity for CFD models.

This paper addresses the comparison of model scale experiments with CFD computations. The analyses were conducted entirely blind, i.e. without reference to the results. Only the geometric data for mesh building was supplied to the analyst. The comparisons discussed below attempt to provide a meaningful analysis. Some care is needed since both the model tests and the computational runs were relatively short.

If the time series was highly modulated, estimates of means and maxima become suspect and an allowance needs to be made for variability introduced by the short runs.

MODEL TESTS

Experiments

Spar VIM is driven by large scale vortices shed from the hull. The experimental program focused on the effect of hull appurtenances and Re scaling on the resulting motions [3]. A truss spar hull was modeled, ignoring the lower truss and riser portion of a full truss spar. The results are applicable to both truss and classic spar geometries. The experiments towed the spar hulls, which were free to move in 6 degrees of freedom. The tow speeds were limited on the upper end by Froude number effects; see Table 4. The primary response was in sway. Surge was characteristically low. Heave, pitch and roll were very small. The CFD modeling therefore focused on 2dof, surge & sway.

Four configurations were tested at DTMB. Their description and reference nomenclature used here is given in Table 1. The CFD mesh name will be used throughout this report. The basic cylindrical hull with three start strakes and all appurtenances (SPCA) is shown in Figure 1. The break in the strakes was introduced to facilitate towing and rotating the models in the towing tank. Figure 2 shows a close-up of the mooring chains and anodes; note the standoffs used for their positioning; these were not modeled. In order to achieve the highest possible Re, a relatively high level of towing tank blockage was accepted; see Table 2. Model particulars are listed in Table 3.

Table 1 - Spar Geometries

CFD Mesh Name	Description
SPCA	Spar with strakes, pipes, chains and anodes
SA	Spar with stakes and anodes
S	Spar with strakes
SPC	Spar with strakes, pipes and chains

Table 2 - DTMB Tank Particulars

Model Dia. [m]	Tank Draft [m]	Tank Width [m]
1.75	2.95	15.2
Tank Depth [m]	**Blockage [area %]**	**Blockage [lateral %]**
6.7	5.0%	11.5%

Figure 1 - Large scale spar hull with all appurtenances (Case SPAC).

Figure 2 - Appurtenance details

Table 3 - DTMB Model Dimensions

Parameter	Value
Diameter, *D*	1.75m
Draft, *H*	2.95m
Strakes	3 start, 13%D height
Mass, *M*	7088.1 kg
Damping ratio, ζ	1.10 %
Critical damping	255.2 kg/s
Temperature	~20.5 deg C
Tn (surge & sway)	2.73 sec
Scale ratio	1:22.3
Global stiffness, *K*	2111.3 N/m
Linear damping, *B*	2.8 kg/s
Roughness, *ks/D*	0.0001

*Nominal vs. Maximum A**

Given a modulated signal, one has to decide which parameters are important. The maximum a/D in the record after truncation of the initial transient, A*max, is useful for extreme estimation. The RMS a/D value might be more appropriate for fatigue related comparisons. As a compromise,

we have elected to make our initial, blind comparisons of the CFD computations for this presentation using the estimated value of the maximum or "nominal maximum", defined as **A*** = √2RMS(a/D). Comparisons using A*max lead to the same conclusions.

Modulation & Repeatability

VIM is typically strongly modulated. The differences between the maximum a/D (A*max) in the record and **A*** is an indicator of the degree of modulation of the time series, assuming initial transients have been adequately excluded. From the 36 cases, (A*max – **A***)/**A*** = 45% for the CFD and 65% from the experiments, indicating that there is a high degree of modulation in many of the records.

The experiments are inherently limited by the length of the tow tank facilities. Duplicate tests were run and most cases were found to be highly repeatable, with **A*** differences usually under 0.05. One exception occurred in one of the experimental cases discussed below (Case SA) when the experiment appeared to have two distinct response states. Bi-stable responses have been seen at low Re [4]. In this situation the VIM response of the straked hull dropped from a very high level to very low with only a few degrees difference in inflow angle. Since the mooring system typically allows a small amount of yaw, the spar can appear to have different response states and might be the source of the anomalous behavior.

The CFD record lengths can in principle be made as long as desired, but generally are cut as short as possible for expediency. Some of the CFD records here are somewhat short and should be extended for more reliable estimates.

Benchmarking Test Cases

The majority of tests were conducted at three reduced velocities, Urn = 6, 7 & 8, see Table 4, and over a large number of directions. The lines connecting the results over the Urn range 6-7-8 in the figures below are to aid the reader in making comparisons. While we believe the general trends are plausible, only the symbols represent actual data.

Table 4 - DTMB case Re & Fr numbers

DTMB Vrn	Velocity U [m/s]	Re	Fr
6	0.640	1.14e6	0.154
7	0.746	1.33e6	0.180
8	0.853	1.52e6	0.206

CFD MODELING

Appurtenances

The simulation of the flow around large spar platforms is made difficult both because of the many large vortex structures that need to be resolved in the flow and because of the complex underwater geometry of the platform. Unlike ships and submarines that have smooth and mostly uninterrupted shapes, most spars are festooned with external pipes, mooring chains and other features that interrupt the flow near the spar and influence points at which the flow separates from the platform. Each of these smaller features or appurtenances has its own complex flow pattern which would require a proportionate fine mesh around the appurtenance and increase the problem size almost as much as adding a new spar. Even with current large computers the numerical solution becomes too large for practical solution under these conditions. It is the premise of this study that this problem can be solved without detailed and expensive resolution of the flow around the appurtenances. This is based on the idea that the main forces causing VIM are the surface tractions on the spar hull and not the appurtenances. Thus the objective of the CFD solution is to predict forces on the hull accurately. Furthermore, errors in predicting the loads on the appurtenances are negligible because these loads are a small fraction of the total load. It is only important that the effect of appurtenances on the hull loads be modeled, such as the way in which they might influence the points of flow separation.

A number of approaches were investigated. A reasonable compromise between accuracy and economy that exhibited the requisite robustness turned out to be the use of a course mesh around the smaller appurtenances. Very complex shapes are further simplified: e.g. chains are modeled as pipes. This method reduces the problem size dramatically and makes solutions practical. The flow around the hull and strakes were modeled with a high degree of fidelity. The pipes, chains and anodes were treated as appendages with a coarser mesh. The supports used for the chains and anodes were ignored and not meshed.

Meshes

In anticipation of this benchmarking opportunity, four meshes were prepared from CAD files, as illustrated in Figure 3. These CAD drawings typically need a fair amount of expert intervention since details are often missing (e.g. brackets and anodes) and the models are rarely watertight, a requirement of most automatic meshing software.

Each mesh had an initial orientation with 180 degrees facing upstream. Three directions (30, 60 & 90 degrees) appeared to be particularly suitable for benchmarking, since they exhibited distinctly different behavior for various appurtenance combinations. The three different inflow direction meshes were prepared by rotating the hull and surrounding cells as a rigid body. The cell density around the hull was unchanged. The boundary layer region was designed for high Re modeling in anticipation of the need to run full scale comparisons. Sample meshes are shown in Figure 4 & Figure 5. Mesh specifications for the most complex geometry are reported in Table 5. This is a large mesh by current standards, but far larger meshes are routinely used. Previous

mesh sensitivity work justified the resolution employed here for the appurtenances. A denser mesh and more a more detailed modeling of the chains is desirable, but could not be justified at this stage of the benchmarking exercise. As the body moved, the dense mesh near the hull was held fixed. The mesh outside this region to the boundaries was stretched/compressed in a linear fashion to accommodate the motion. The larger cells in the far field are in areas of small gradients and achieve a balance between accuracy and problem size.

Figure 3 - 3D view of the truss spar hull CAD drawing (Case SPC)

Table 5 - Sample mesh specifications

Mesh Specification	Case SPCA
Total Number of Nodes	1,851,697
Total Number of Elements	5,644,747
Number of Wedge Elements (Boundary Layer)	2,407,732
Number of Tet Elements (elsewhere)	3,237,015

CFD Code & Turbulence Models

The finite element code AcuSolve™ was used for all of the CFD computations. The initial blockage studies used a RANS S-A turbulence model. All of the benchmark cases reported here used Spalart's "delayed" detached-eddy simulation (DDES) turbulence model [5], unless noted. DDES is a variant on DES, which effectively uses a RANS model near the wall and LES out in the fluid. For the problems investigated to date, DDES and DES have given similar results. DDES does ensure a consistent RANS-LES transition and is recommended. AcuSolve™ and DES have proven to be robust, provide high resolution and are efficient. The DTMB comparisons are at the supercritical Re, avoiding any low Re turbulence modeling issues.

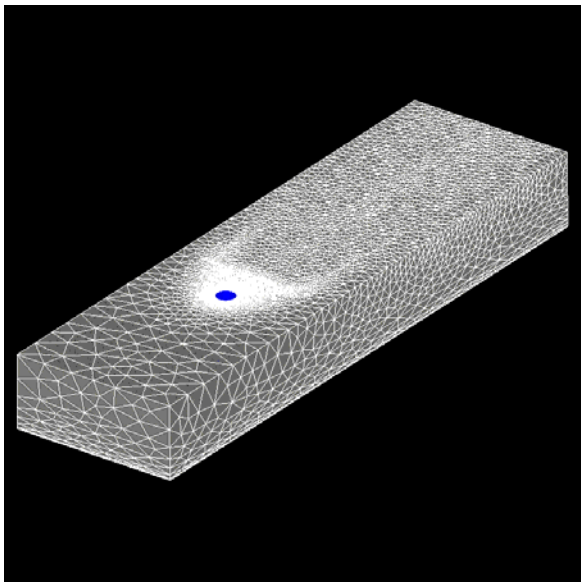

Figure 4 - Mesh for the DTMB tank.

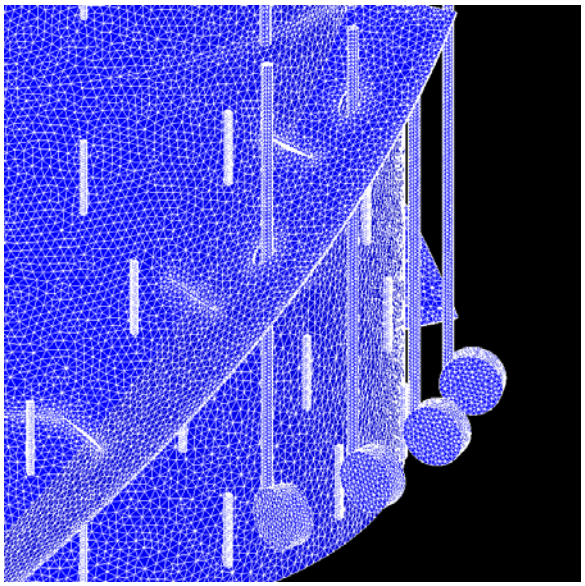

Figure 5 - Sample mesh for case SPCA

Spar Equations of Motion & BCs

The experiments were conducted at low Froude numbers and the motions were primarily surge and sway. Therefore the free surface was modeled as a rigid, free-slip surface and the equations of motions for the spar were limited to the horizontal plane:

$$Mx'' + Bx' + Kx = F_{hx}$$
$$My'' + By' + Ky = F_{hy}$$

For all of the blind benchmark tests, the linear damping term B was set to zero. The upstream boundary used an inflow condition of the model speed. The tank side and bottom walls were modeled as a free-slip since the model was towed and there was no flow along the walls. A simple outflow boundary condition, integral of pressure = 0, was used at the back of the modeled tank.

Roughness & Wall Functions

Since both full-scale spars and the models tend to have some degree of roughness, adjusted wall functions are used. This also reduces the mesh density requirements. The roughness was estimated to be ks/D=0.0001. The y+ values are in the 30-100 range.

Parameter Sensitivity

The CFD benchmarks were run without any mechanical damping. The experiments, on the other hand, could not prevent the introduction of damping from the towing/mooring systems. In order to check the effect of external damping, one of the cases showing a larger difference between the CFD and the measurements was re-run with 2% mechanical damping. For the case shown in Table 6, **A*** dropped from 0.8726 to 0.8249 or 5.5%. The 2% value appears to be high relative to the DTMB experimental decay tests. The total damping, mechanical and hydrodynamic, derived experimentally from the DTMB decay tests was estimated to be on the order of 1.1% of critical. The inclusion of mechanical damping in the CFD analysis would therefore probably only reduce the estimates by a few percent. Changing the time step yielded only a 0.5% drop.

Table 6 - Parameter Sensitivity, SPCA, 30deg, Vrn=8

A*	dt [sec]	% damping
0.8726	0.3	0%
0.8249	0.3	2%
0.8680	0.1	0%

Hardware & Time Steps

In order to simulate 25 spar oscillations, or 365 sec at model scale, a time step of 0.3 sec was used requiring 1250 time steps. The computational time required was 27 hrs for the 1250 steps or 80 seconds per time step on a 32 CPU Intel Xeon 3 GHz cluster with a Gigabit switch connectivity. Though this cluster is somewhat larger than ones currently available to most engineers, it pales when compared to the size of clusters routinely used in seismic and aerospace investigations. If speed is required, increased computer power can be acquired. Post processing can be highly automated for production runs. Delays associated with project definition, funding and acquiring the necessary input data are more of a problem than the length of the individual runs. Important information can be extracted progressively and the program easily altered day-to-day to accommodate changing needs. Hence the total number of runs times the individual run time need not be the limiting factor on whether to perform a CFD analysis.

For this problem set, 70% of the run time was utilized by CPU operations and 30% by network communications between CPUs. The total RAM memory requirement for this problem was 5 Gb. The convergence criteria were set automatically by the AcuSolveTM auto solution strategy. The flow field and turbulence solution were staggered, but run twice per time step to achieve higher accuracy. At the second call of the stagger the solution from the first set of iterations is feed back for a second set of iterations. The flow stagger required 60-80 iterations to converge and the turbulence stagger about 10 iterations, the minimum number of allowed iterations.

CFD BENCHMARKING

Case S

Figure 6 presents the results (nominal maxima, **A***) when strakes (S) are the only appendages. We expect the strakes to work at their optimal performance. While the response is low, there is some directional dependence, probably due to low strake coverage at the 90deg inflow direction. The blind CFD results appear to follow the experimental results exceptionally well and are slightly conservative, i.e. slightly overestimate the experiments, possibly since no damping due to the test rig was included. The mesh is an accurate representation of the experimental setup. Figure 8 illustrates the flow around the spare in terms of the z-vorticity. The strakes appear to control the regions of separation. A sample time series from both the CFD and the experiments is given in Figure 13.

Case SPCA

Figure 7 presents the nominal maxima results for strakes plus all appurtenances: pipes, chains & anodes (SPCA). Here again the blind CFD results appear to follow the experimental results reasonably well. The response is far larger than for the strakes alone (Case S), suggesting that the appurtenances severely reduce the effectiveness of the strakes. Here the model is less faithful to the experimental setup. The local mesh for the pipes, chains and anodes is relatively coarser than for the hull and strakes, a compromise for computational expediency. Also, damping due to the mooring system in the experiments has not been included in the CFD model. Figure 9 illustrates the flow around the spar with all appurtenances. This is also in terms of the z-vorticity and should be compared with Figure 8. The two illustrations are as near to the same flow conditions and offsets as possible. The differences in flow patterns and separation character are evident. The pipes and anodes appear to trip a separation line along the hull, resulting in far more motions than for the strakes alone. A sample time series from both the CFD and the experiments is given in Figure 14.

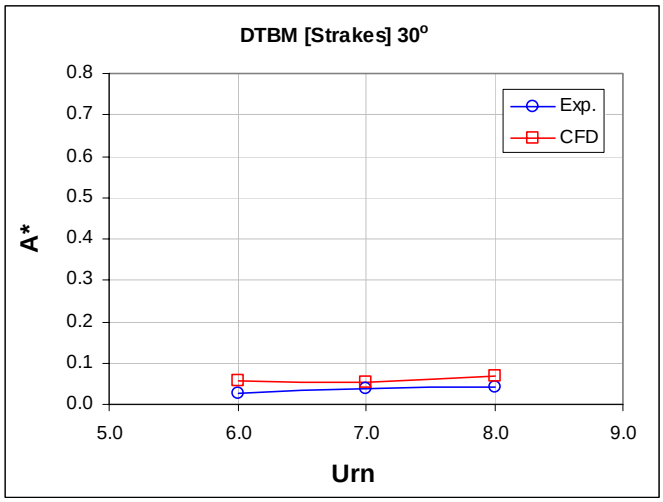

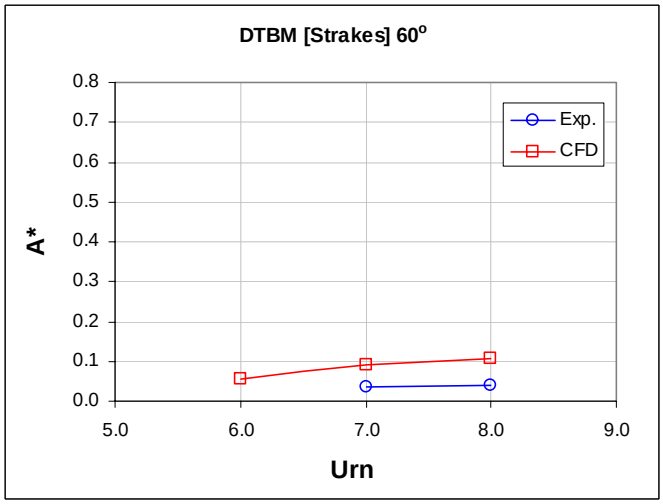

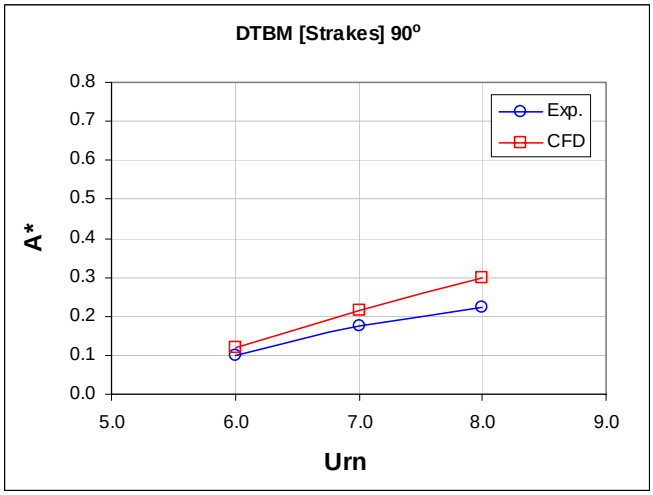

Figure 6 - Case S: Experiments & CFD at 30, 60 & 90 degrees; nominal maximum in record

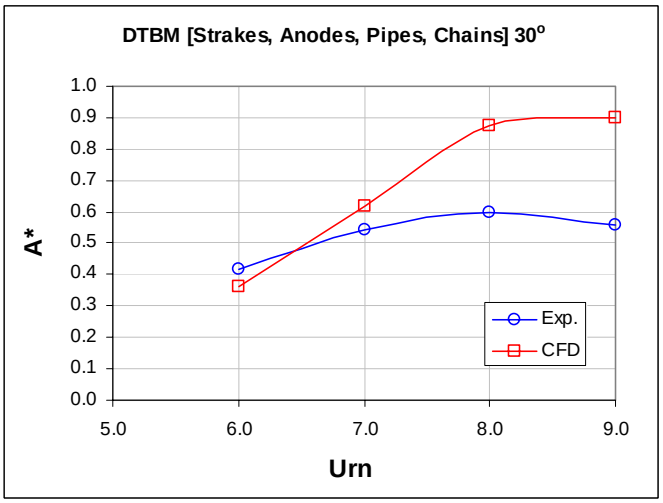

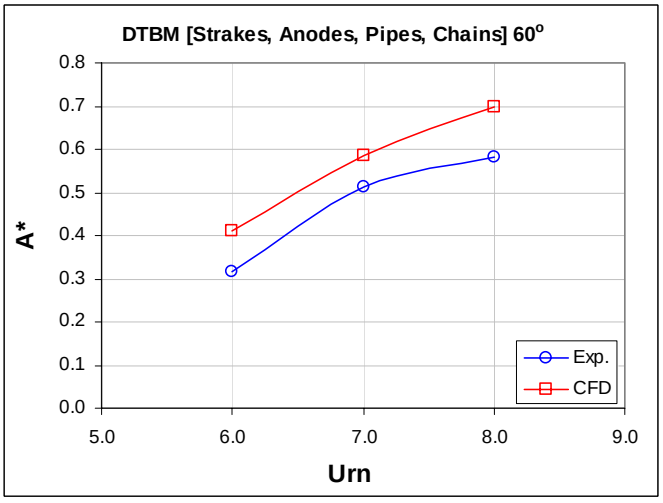

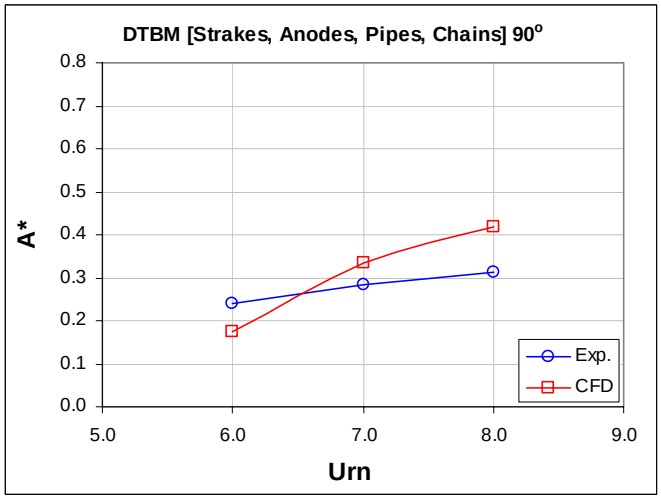

Figure 7 - Case SPCA: Experiments & CFD at 30, 60 & 90 degrees; nominal maximum in record

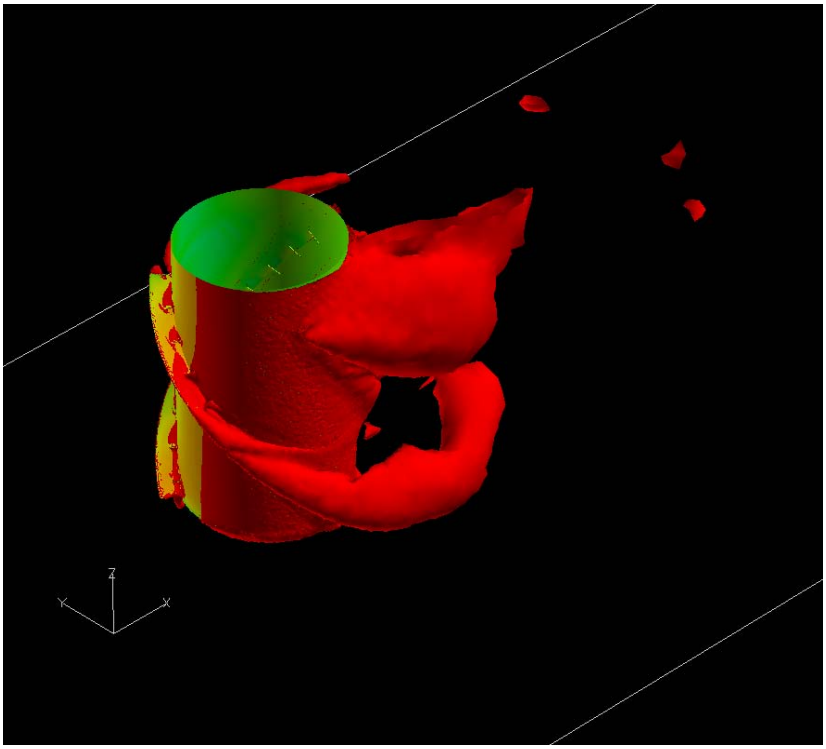

Figure 8 - Case S: Vorticity at Urn=8 showing regions of separation controlled by the strakes

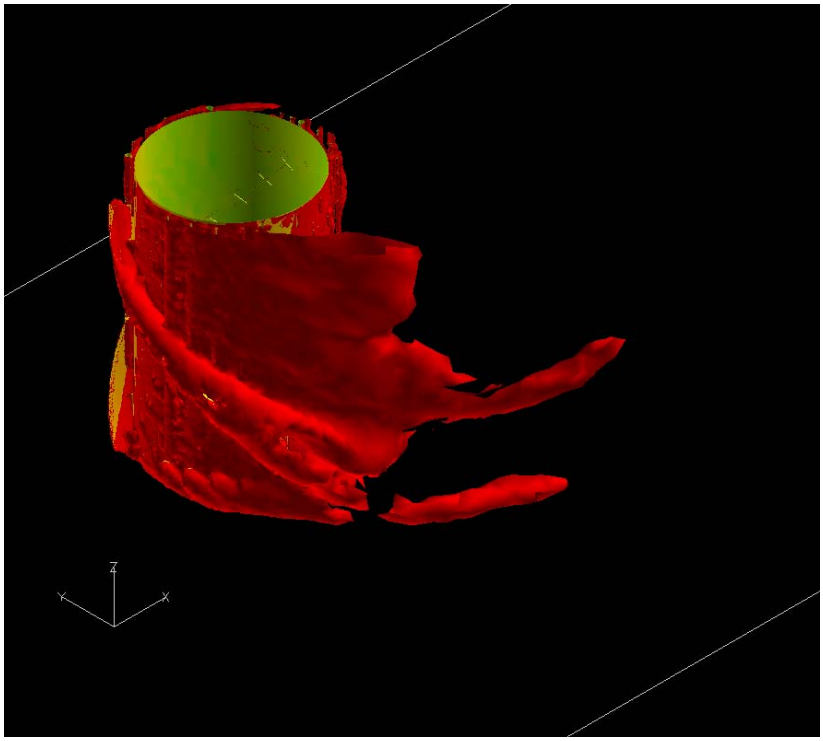

Figure 9 - Case SPCA: Vorticity at Urn=8 showing regions of separation controlled by the strakes and off the cylinder by the pipes, chains and anodes.

Case SPC

In an effort to understand the effect of various types of appendages, experiments were conducted with the anodes removed, leaving the strakes, pipes and chains (SPC) as appendages. If the response fell dramatically, it might be possible to achieve the intended corrosion protection in another way than using this type of external anode. Note that **A***, Figure 10, is considerably larger than for the case of strakes alone (S). Clearly the pipes and chains have a significant effect. The CFD results capture this change in the hydrodynamics and appear to follow the experimental results at 30. At 60 degrees, the experimental records have maxima that trend closer to the CFD predictions at *Vrn* of 7 and 8. Repeat experimental runs showed a large degree of variability and were highly modulated. The 90 deg case appears anomalous in that this was the only case where the CFD results fell consistently below the measurements.

Case SA

Another test looked at strakes and anodes alone (SA); see Figure 11. Anodes alone alter the flow around the spar in a different fashion than the long vertical pipes & chains. This is a test of a CFD model mesh that does not exactly match the anode geometry (the standoffs were not modeled) and the mesh around the anodes is relatively coarse.

As noted earlier, repeat experimental runs were in close agreement except for a few cases and particular headings. One example is the 30 degree SA case that included some repeat runs with significantly differing levels of response. Note that the response dropped drastically from high values at 30 degrees to low values at 40 degrees. At Urn=7 in particular, there were two distinct response levels. The CFD estimate appears to be in the middle, but is likely to come up if the run was longer, as would the Urn=6 case. The 60 degree CFD runs severely overestimate the experimental values. In the 40-80 degree range, the experiments showed low responses, so this is not a case where a small rotation would make a big difference. It is not clear why the CFD overestimated. A finer mesh might improve the benchmarking, albeit at the cost of extra computational effort. At 90 degrees, on the other hand, the CFD and experimental values agree well.

Appurtenance Overview

Another view of the CFD data illustrates the impact of the various appurtenances and their combination. Here we plot in Figure 12 the four cases, again at 30, 60 & 90 degrees, using the nominal maximum **A*.** The cumulative effect of the appurtenances is evident. The pipes & chains are seen to be the biggest contributor. This is an example of how CFD can assist in evaluation of the impact of design changes.

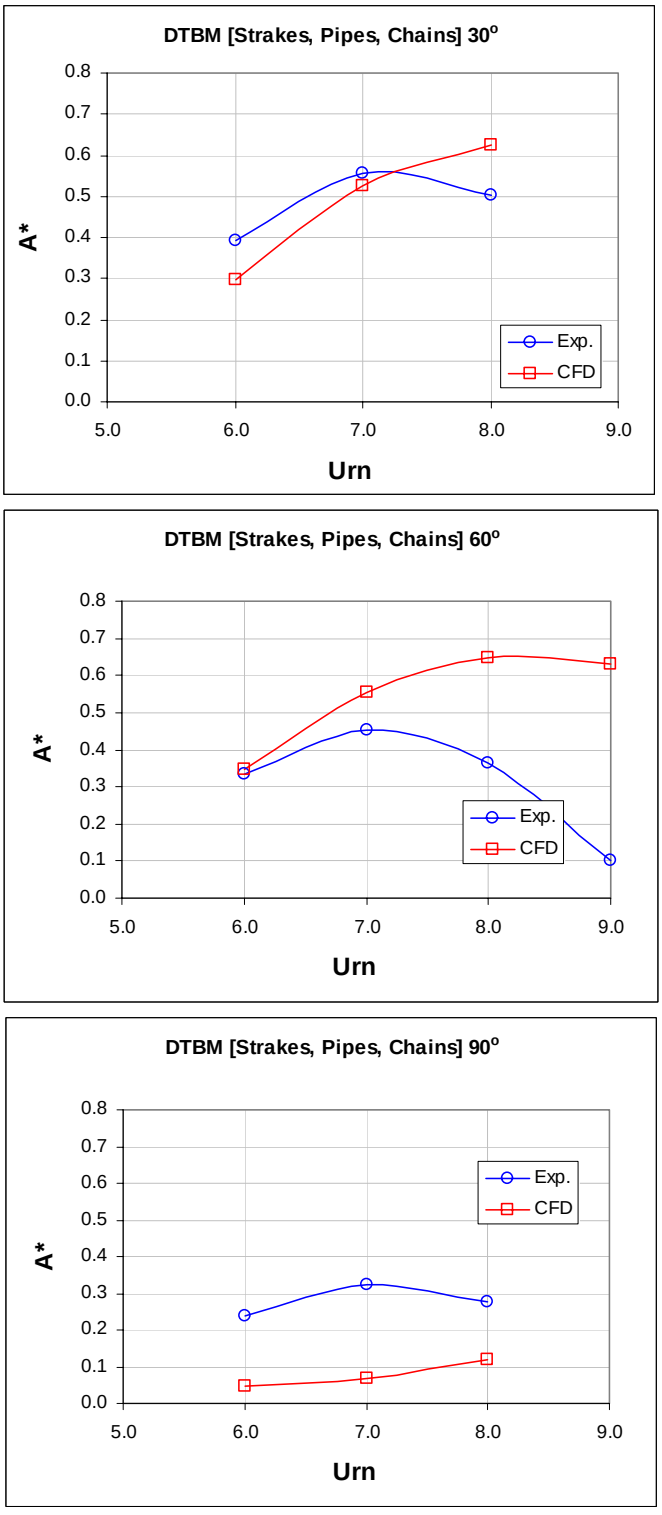

Figure 10 - Case SPC: Experiments & CFD at 30, 60 & 90 degrees; nominal maximum in record

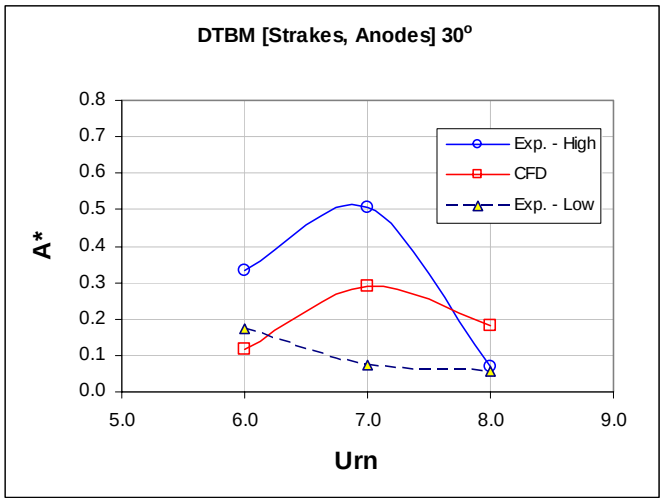

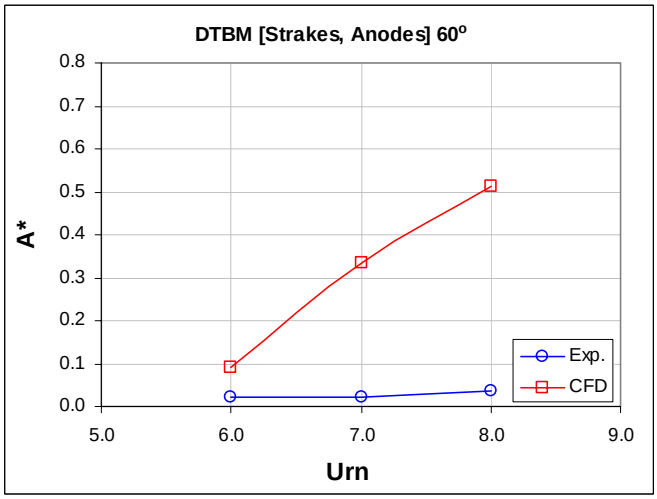

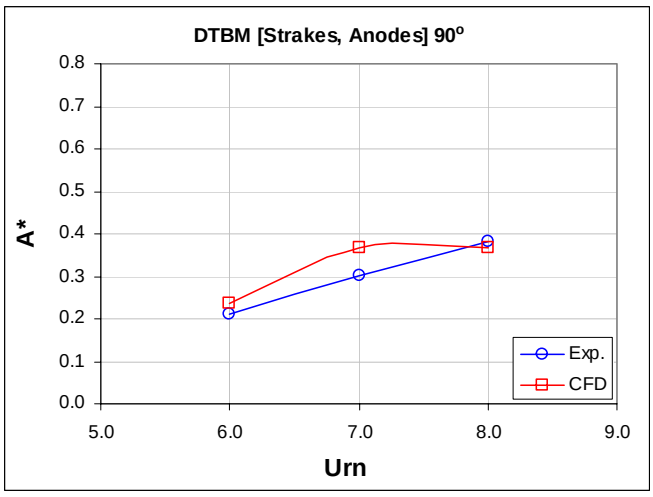

Figure 11 - Case SA: Experiments & CFD at 30, 60 & 90 degrees; nominal maximum in record

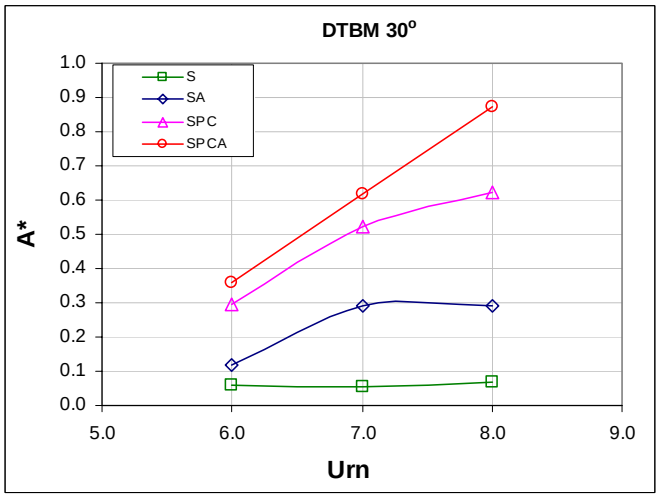

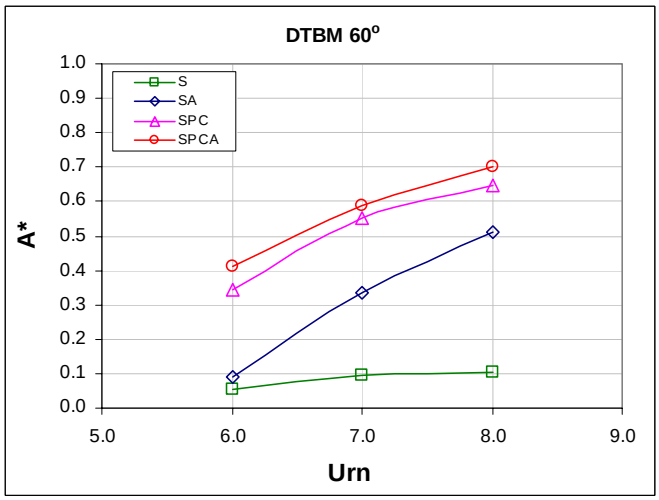

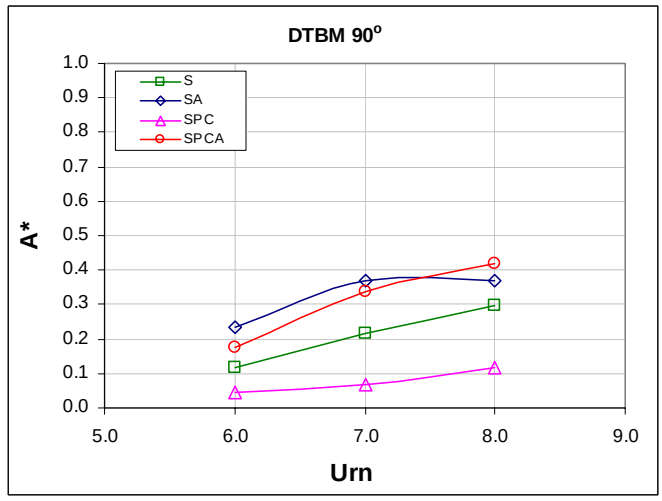

Figure 12 – All CFD Cases at 30, 60 & 90 degrees; nominal maximum in record

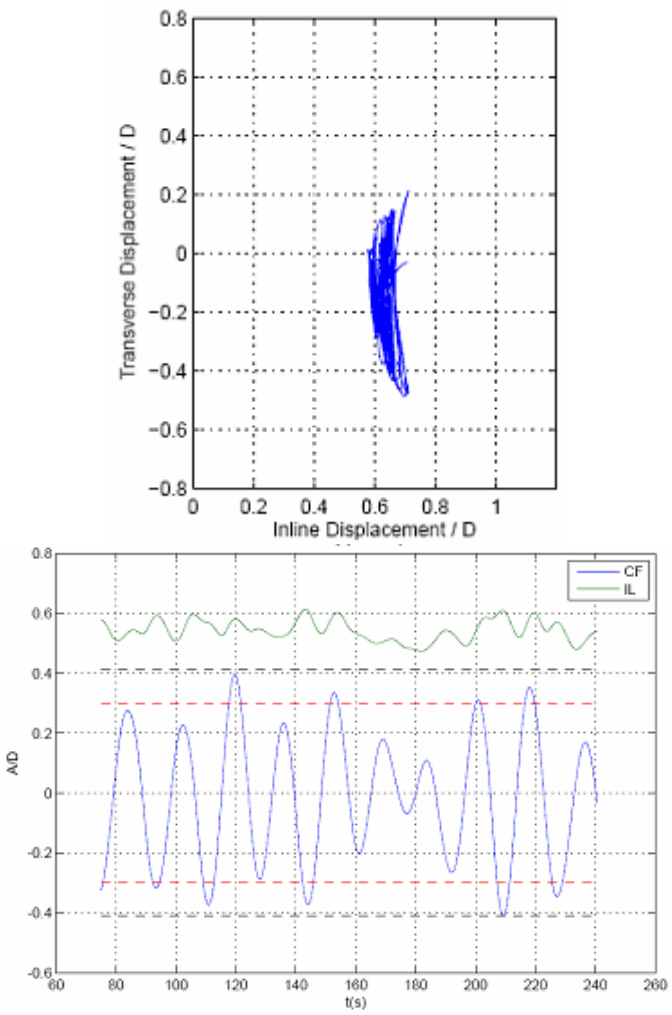

Figure 13 - Case SP, Vrn=8, 90 degrees: experiment (top) and CFD (bottom).

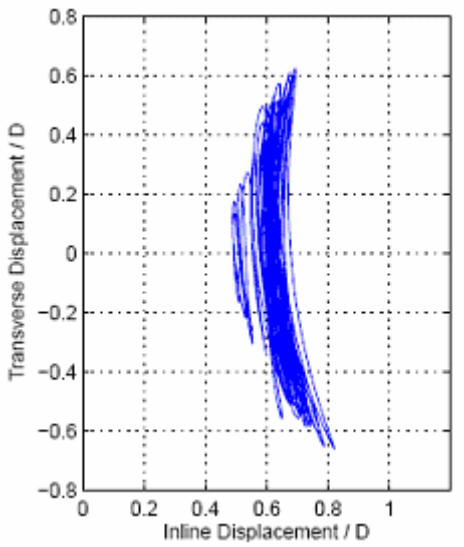

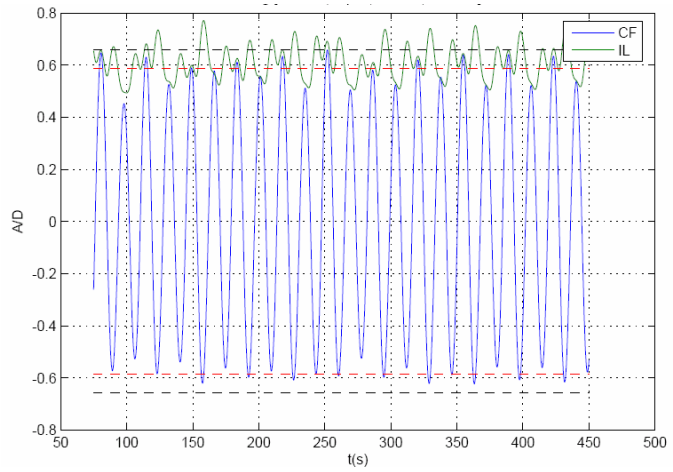

Figure 14 - Case SPCA, Vrn=7, 60 degrees: experiment (top) and CFD (bottom).

CONCLUSIONS & RECOMMENDATIONS

The following conclusions and recommendation are drawn from the above:

- Basic, blind benchmarks (S & SPCA) agreed well with experiments, yielding the correct physics and generally were slightly conservative.
- Fidelity is very important; the more accurate the model, the better the comparison.
- Further refinement of the anode modeling might improve the confidence of CFD estimates, but the effort may not be worth the cost at present.
- The role and estimation of damping needs further study, but appeared to play a small role in these comparisons.

Smaller time steps (dt), mesh refinement and inclusion of the correct amount of external damping would likely bring these results even closer into alignment. We believe that these benchmarks provide a strong basis for the inclusion of CFD modeling in the design and evaluation process for large, offshore structures.

NOMENCLATURE

a = motion amplitude time series, e.g. sway $y(t)$
$\boldsymbol{A^*}$ = nominal nondimensional maximum, $\sqrt{2}*RMS(a/D)$
A^*max = nondimensional maximum A^* in a time record
B = linear damping
D = spar diameter
fn = natural frequency from pluck test
K = spring constant
F_{hx}, F_{hy} = CFD hydrodynamic forces in the (x,y) dir.
M = mass of spar
U = current velocity or tow speed
Urn = nominal reduced velocity, U/fnD

REFERENCES

[1] Halkyard, J., S. Sirnivas, Y. Constantinides, O. Oakley, & K. Thiagarajan, 2005, "Benchmarking of Truss Spar Vortex Induced Motions Derived from CFD with Experiments", *Proc. of the 24th Int. OMAE Conf.*, OMAE2005-67252.

[2] Oakley, O., Y. Constantinides, C. Navarro, & S. Holmes, 2005, "Modeling Vortex Induced Motions of Spars In Uniform and Stratified Flows", *Proc. of the 24th Int. OMAE Conf.*, OMAE2005-67238.

[3] Finnigan, T. & D. Roddier, 2007, "Spar VIM Model Tests at Supercritical Reynolds Numbers", Proc. *of the 26th Int. OMAE Conf.*, OMAE2007-29160.

[4] Williamson, C.H.K. & N. Jauvtis, 2004, "A high-amplitude 2T mode of vortex-induced vibration for a light body in XY motion", *European Journal of Mechanics B/Fluids* 23, pp 107–114.

[5] Spalart, P.R., S. Deck, M.L. Shur, K.D. Squires, M.Kh. Streletes & A. Travin, 2005, "A New Version of Detached-Eddy Simulation, Resistant to Ambiguous Grid Densities", *Theoretical & Computational Fluid Dynamics.*

ACKNOWLEDGEMENTS

The meshes and model setup were performed with the assistance of Dr. Samuel Holmes (Red Wing Engineering). Tim Finnigan (Chevron) and Dr. Dominique Roddier (MI&T) helped provide the experimental data. All of the CFD runs were made in-house by Yiannis Constantinides. The assistance of all concerned is gratefully acknowledged.